


## Article

# Structure-Properties Correlation of Cross-Linked Penicillin G Acylase Crystals

Marta Kubiak <sup>1,†</sup>, Janine Mayer <sup>2,†</sup>, Ingo Kampen <sup>1</sup>, Carsten Schilde <sup>1</sup> and Rebekka Biedendieck <sup>2,\*</sup> 

<sup>1</sup> Institute for Particle Technology, Technische Universität Braunschweig, Volkmaroder Str. 5, 38104 Braunschweig, Germany; marta.kubiak@tu-braunschweig.de (M.K.); i.kampen@tu-braunschweig.de (I.K.); c.schilde@tu-braunschweig.de (C.S.)

<sup>2</sup> Institute of Microbiology and Braunschweig Integrated Centre of Systems Biology (BRICS), Technische Universität Braunschweig, Rebenring 56, 38106 Braunschweig, Germany; janine.mayer@tu-bs.de

\* Correspondence: r.biedendieck@tu-braunschweig.de; Tel.: +49-531-391-55291

† These authors contributed equally to the work.

**Abstract:** In biocatalytic processes, the use of free enzymes is often limited due to the lack of long-term stability and reusability. To counteract this, enzymes can be crystallized and then immobilized, generating cross-linked enzyme crystals (CLECs). As mechanical stability and activity of CLECs are crucial, different penicillin G acylases (PGAs) from Gram-positive organisms have proven to be promising candidates for industrial production of new semisynthetic antibiotics, which can be crystallized and cross-linked to characterize the resulting CLECs regarding their mechanical and catalytic properties. The greatest hardness and Young's modulus determined by indentation with an atomic force microscope were observed for CLECs of *Bacillus* species FJAT-PGA CLECs (26 MPa/1450 MPa), followed by BmPGA (*Priestia megaterium* PGA, 23 MPa/1170 MPa) and BtPGA CLECs (*Bacillus thermotolerans* PGA, 11 MPa/614 MPa). In addition, FJAT- and BtPGA CLECs showed up to 20-fold higher volumetric activities compared to BmPGA CLECs. Correlation to structural characteristics indicated that a high solvent content and low number of cross-linking residues might lead to reduced stability. Furthermore, activity seems to be restricted by small water channels due to severe diffusion limitations. To the best of our knowledge, we show for the first time in this study that the entire process chain for the characterization of diverse industrially relevant enzymes can be performed at the microliter scale to discover the most important relationships and limitations.

**Keywords:** penicillin G acylase (PGA); immobilization; cross-linked enzyme crystal (CLEC); micromechanics; atomic force microscope; catalytic activity



**Citation:** Kubiak, M.; Mayer, J.; Kampen, I.; Schilde, C.; Biedendieck, R. Structure-Properties Correlation of Cross-Linked Penicillin G Acylase Crystals. *Crystals* **2021**, *11*, 451. <https://doi.org/10.3390/cryst11040451>

Academic Editor: Abel Moreno

Received: 29 March 2021

Accepted: 19 April 2021

Published: 20 April 2021

**Publisher's Note:** MDPI stays neutral with regard to jurisdictional claims in published maps and institutional affiliations.



**Copyright:** © 2021 by the authors. Licensee MDPI, Basel, Switzerland. This article is an open access article distributed under the terms and conditions of the Creative Commons Attribution (CC BY) license (<https://creativecommons.org/licenses/by/4.0/>).

## 1. Introduction

Penicillin G acylases (PGAs; EC 3.5.1.11) are key enzymes for the biotechnological production of  $\beta$ -lactam antibiotics in the pharmaceutical industry [1]. Notwithstanding the early discovery of penicillin in the 1920s by Alexander Fleming,  $\beta$ -lactam antibiotics still represent the most widely used antibiotic class today [1,2]. PGAs are heterodimeric enzymes applied for the hydrolysis of natural penicillin G, yielding 6-aminopenicillanic acid (6-APA) as an important precursor for synthesis of semisynthetic  $\beta$ -lactam antibiotics such as ampicillin or amoxicillin. Furthermore, PGAs can catalyze the synthesis of these semisynthetic  $\beta$ -lactam antibiotics by condensation of activated acyl donors to  $\beta$ -lactam precursors such as 6-APA [1]. Due to increasing microbial resistance, new semisynthetic  $\beta$ -lactam antibiotics produced by PGA are developed to overcome microbial resistances [3].

PGAs are ubiquitous; they are found in fungi, yeast and bacteria. In industry, PGAs from Gram-negative bacteria such as *Escherichia coli* (EcPGA) or Gram-positive bacteria such as *Priestia megaterium* (formerly known as *Bacillus megaterium*) (BmPGA) are mainly used [4,5]. Recently, two novel PGAs from Gram-positive *Bacillus thermotolerans* (BtPGA) and *Bacillus sp.* FJAT-27231 (FJAT-PGA) were discovered. Compared to commonly used

PGAs from *P. megaterium* and *E. coli*, they show significantly improved thermal stability and activity for the hydrolysis of penicillin G yielding 6-APA [6], making them promising candidates for use in a potential biocatalytic process to obtain precursor molecules for synthesis of semisynthetic antibiotics. Their enzymatic synthesis is usually preferred to chemical synthesis due to efficiency and selectivity of enzymes under mild reaction conditions without hazardous chemicals and solvents. However, free enzymes often lack long-term stability and reusability. To counteract these problems, one option, among others, is to immobilize enzymes. A possibility for carrier-less immobilization of enzymes is the production of cross-linked enzyme crystals (CLECs) [7]. After enzyme crystallization in aqueous buffer conditions at optimal pH, the crystals are covalently cross-linked by addition of bifunctional reagents, usually glutaraldehyde. The resulting CLECs can provide robust and highly active immobilized biocatalysts. Due to the absence of a carrier, the production of CLECs is inexpensive. Further, CLECs show high space–time yields and productivities due to the high enzyme load [7].

The catalytic activity of CLECs correlates with their particle size [8,9]. Therefore, the knowledge of mechanical properties of CLECs is essential for designing a process to avoid breakage and ensure constant particle size distribution and thereby constant process conditions. Until now, there are just few publications about mechanical properties of protein crystals (Table S1). In the past two decades, researchers have studied the dependency of micro-Vickers hardness of native lysozyme crystals on intracrystalline water [10–13] and reported values of micro-Vickers hardness ranging from 2 to 20 MPa for wet tetragonal lysozyme crystals [10,11,13] and from 6 to 10 MPa for anisotropic crystal faces of orthorhombic hen egg-white lysozyme [12]. The increase in hardness of dry lysozyme crystals by at least one order of magnitude is described to be related mainly to the dislocation mechanism [10–13]. Tait et al. (2008) examined mechanical properties of protein crystals using a nanoindentation method and found hardness of native wet lysozyme crystals to be about 15 MPa with a Young's modulus of around 490 MPa [14]. Morozov and Morozova (1981) pioneered the measurements of the Young's modulus of native and cross-linked triclinic lysozyme crystals with a mechanical resonance technique. They measured the Young's modulus in the range of 290 to 1400 MPa, which was not significantly affected by the cross-linking [15]. Kubiak et al. (2018) measured hardness and Young's modulus of different CLECs using an atomic force microscope (AFM)-based nanoindentation technique. The determined differences in the mechanical behavior of distinct cross-linked protein crystals were correlated with the different crystal structures and properties [16]. Furthermore, the authors identified an anisotropic mechanical behavior of halohydrin dehalogenase HheG crystals, caused partly by the crystal structure and partly by the cross-linking time [17]. The cross-linking time influences not only the micromechanical properties of the biocatalysts but also the catalytic activity. Margolin (1996) reported that mechanical stability increases with increasing cross-linking degree, but excess cross-linking can lead to protein precipitation and loss of activity [8].

In our study, CLECs from different promising penicillin G acylases (PGAs) were mechanically and catalytically characterized. In order to correlate the CLEC properties with its structure, a process chain was designed, starting with enzyme production and purification, particle synthesis and mechanical measurements by AFM-based nanoindentation. The distinct mechanical properties, such as indentation hardness and Young's modulus, of FJAT-, Bt- and BmPGA CLECs as well as their catalytic activity were investigated and the measured differences were finally analyzed based on the enzyme structure. As far as we know, this is the first study focusing on the entire small-scale process chain for the production and characterization of industrially relevant enzymes. Therefore, this project makes a major contribution to design of CLECs, showing the most important relationships and limitations.



## 2. Materials and Methods

### 2.1. Recombinant Protein Production

FJAT- and BtPGA, which were recently identified, as well as the already known BmPGA, were recombinantly produced and secreted with *P. megaterium* MS941 via plasmids pRBBm316, pRBBm311 and pALBm1, respectively [6,18,19]. For each, LB medium (10 g/L tryptone, 5 g/L yeast extract, 5 g/L NaCl) supplemented with 10 mg/L tetracycline and 2.5 mM CaCl<sub>2</sub> (Bt- and BmPGA) was inoculated with an overnight culture and cultivated at 37 °C and 200 rpm in baffled flasks. At OD<sub>578</sub> of 0.3 to 0.4, the recombinant protein production was induced by addition of 0.5% (*w/v*) xylose. After further cultivation for 22 h, the cell-free supernatants containing the secreted PGAs were obtained by centrifugation (3345 × *g*, 20 min, 4 °C) and sterile filtration (0.22 μm) for subsequent protein purification.

### 2.2. Protein Purification

FJAT- and BmPGA were purified by cation and BtPGA by anion exchange chromatography from the cell-free supernatant followed by preparative gel permeation chromatography, as described previously [6]. Fractions with the respective PGAs were combined and concentrated using Amicon centrifugal filters MWCO 10,000 (Merck Millipore, Darmstadt, Germany). Protein concentrations were determined by Bradford assay [20].

### 2.3. Crystallization

PGA crystals were obtained by sitting drop vapor diffusion method. For this, the PGA stock solutions were dialyzed against 10 mM HEPES (pH 7.0). For crystallization experiments PGA solutions of 10 mg/mL for FJAT-PGA, 6 mg/mL for BtPGA and 5 mg/mL for BmPGA were used. For the sitting drop vapor diffusion crystallization, 10 μL droplets were placed on siliconized cover slides (Jena Bioscience, Jena, Germany). Cover slides and a 1 mL reservoir with the corresponding crystallization buffer for each PGA were placed in Petri dishes, sealed and kept at 17 °C.

For FJAT-PGA, crystal growth was achieved in droplets consisting of 4 μL FJAT-PGA solution (10 mg/mL), 4 μL FJAT-PGA crystallization buffer (8% (*w/v*) PEG 8000 in 100 mM HEPES pH 7.5) and 2 μL FJAT-PGA crystal seed suspension. BtPGA crystals were obtained after mixing 4 μL BtPGA solution (6 mg/mL), 4 μL BtPGA crystallization buffer (20 mM calcium chloride, 100 mM sodium acetate (pH 4.6), 30% (*v/v*) MPD (2-methyl-2,4-pentanediol), pH 5.57) and 2 μL BtPGA seed suspension. BmPGA crystals were developed from droplets containing 4 μL BmPGA solution (5 mg/mL), 4 μL BmPGA crystallization buffer (200 mM potassium iodide, 20% (*w/v*) PEG 3350) and 2 μL BmPGA seeds diluted in a buffer containing 200 mM magnesium chloride and 20% (*w/v*) PEG 3350.

### 2.4. Production of Crystal Seeds

Crystal seeds were prepared from already grown crystals by fragmentation and used as nucleation seeds for further crystallization approaches. For this, crystals in a 10 μL droplet were crushed and transferred with a pipette tip into a 1.5 mL reaction vessel. An amount of 40 μL of crystallization buffer and a HR-320 PTFE seed bead (Hampton Research, Aliso Viejo, USA) were added. The mixture was stirred for 30 s using a vortex mixer and then kept on ice for 30 s. The mixing and cooling procedures were repeated five more times. Then, seed suspensions with increasing dilutions of up to 100X were prepared. The crystal seed suspensions were directly used or stored at −80 °C.

### 2.5. Generation of Cross-Linked Enzyme Crystals (CLECs)

To stabilize the enzyme crystals, they were covalently cross-linked by glutaraldehyde. Prior to cross-linking, the crystal droplets were cooled on ice for 30 min to prevent osmotic shock and bursting of the crystals. The mother liquor was then removed from the crystals and the crystals were washed several times with 5 to 10 μL of the appropriate crystallization buffer. An amount of 10 μL of cross-linking solution consisting of the corresponding

crystallization buffer with 5% (*v/v*) glutaraldehyde was added to the crystals and incubated at 4 °C for 24 h. Subsequently, the CLECs were washed again.

## 2.6. Mechanical Measurements

Due to atomic force microscope (AFM)-based nanoindentation, the influence of viscoelastic behavior of protein crystals on creeping motion during a measurement can be considerably reduced [16,21]. Hence, AFM (JPK NanoWizard3<sup>®</sup>) was used to determine hardness and Young's modulus of PGA CLECs according to the Oliver and Pharr theory [22]. All indentation tests were carried out in force spectroscopy mode in liquid environment and at room temperature. For the measurement, a cantilever with a spherical tip having a radius of 300 nm and a nominal spring constant of 40 N/m (Biosphere, nanotools, München, Germany) was applied. At the beginning of the measurement the cantilever was calibrated on a glass substrate in order to calculate its exact spring constant and sensitivity. Then, a sample with crystals was placed in the measurement area of the AFM. With the aid of an optical microscope, an appropriate crystal (crystal face, which was orthogonal aligned to the cantilever) was chosen and placed under the cantilever. For each crystal, an individual indentation grid with approximately 18 different coordinates was set on the crystal surface and the cantilever was positioned above the first measurement point. A preload of 100 nN was set for surface detection. After the surface was detected, the cantilever retracted 1 µm and was in standby mode. From this position, an indent was carried out with an indentation speed of 2 µm/s until an indentation force of 250 nN was reached. This way, AFM load–displacement curves consisting of baseline, loading and unloading curves were obtained, as shown in Figure 1. Between measurements at different coordinates, it was necessary to retract the cantilever another 15 µm so that the cantilever tip was not destroyed on any surface roughness.

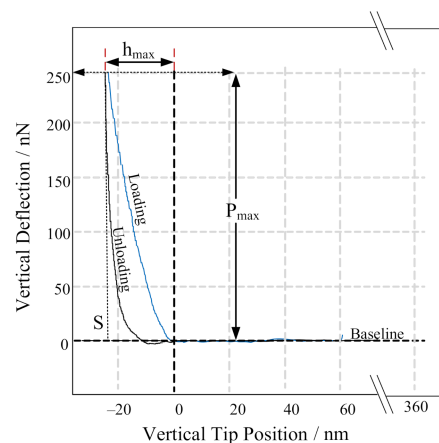


**Figure 1.** Representative force–displacement curve of an AFM-based nanoindentation showing important measurement parameters.  $P_{max}$  = peak load (nN);  $h_{max}$  = maximal depth at the peak load (nm);  $S$  = slope of unloading curve. Reprinted with permission from [17]. Copyright (2019) American Chemical Society.

Adapting the calculation method of Oliver and Pharr to the force–displacement curves measured with the AFM, the necessary key parameters (the peak load  $P_{max}$ , the depth at the peak load  $h_{max}$  and the slope of unloading curve  $S$ ) can be extracted (Figure 1). The contact point, indentation depth and slopes of the unloading curves were obtained and processed with the help of MATLAB2017a.

Hardness  $H$  was determined according to Equation (1), where  $A_c$  is the projected area. For a spherical indenter tip, the area was calculated following Equation (2).

$$H = \frac{P_{max}}{A_c} \quad (1)$$

$$A_c = 2 \cdot \pi \cdot R \cdot h_c - \pi \cdot h_c^2 \quad (2)$$

With knowledge of the indenter tip geometry, the contact depth  $h_c$  can be calculated using Equation (3), where  $\varepsilon$  is a geometric constant. For a spherical indenter tip,  $\varepsilon$  is noted to 0.75 [23].

$$h_c = h_{max} - \varepsilon \frac{P_{max}}{S} \quad (3)$$

The reduced Young's modulus can finally be calculated according to Equation (4).

$$E_r = \frac{\sqrt{\pi}}{2} \cdot \frac{S}{\sqrt{A_c}} \quad (4)$$

Calculated hardness and Young's modulus were plotted as a cumulative distribution for each of the crystal faces in order to identify any differences on single crystal faces. Then, the results of crystal slurries were summarized for different CLECs. A total of 310 measurements on BmPGA CLECs, 284 on BtPGA CLECs and 170 on FJAT-PGA CLECs were used to plot the cumulative distributions.

### 2.7. NIPAB Assay for Activity Determination of PGA CLECs

For determination of PGA activity, an assay based on the hydrolysis of the substrate analog 2-nitro-5-[(phenylacetyl)amino]-benzoic acid (NIPAB, Sigma Aldrich, St. Louis, USA) was used. Cleavage of NIPAB by PGAs releases the dye 2-nitro-5-aminobenzoic acid (NABA), which absorbs at 405 nm. For activity determination, the PGA CLECs from one droplet stored in 10  $\mu$ L 10 mM HEPES (pH 7.0) were rinsed from the cover slide into a flat-bottom microtiter plate using 90  $\mu$ L substrate solution (600 mg/L NIPAB in 9.4 mM  $\text{NaH}_2\text{PO}_4$  and 40.6 mM  $\text{Na}_2\text{HPO}_4$ , pH 7.5). After mixing for 10 s, the absorbance (A) at 405 nm was measured at 37  $^\circ\text{C}$  using the microplate reader (NanoQuant infinite M200 pro, Tecan, Männedorf, Switzerland) 30 times every 10–20 s with mixing for 5 s after every 2nd cycle. For activity determination of soluble enzyme, 90  $\mu$ L NIPAB substrate solution and 10  $\mu$ L purified PGA were mixed and the absorbance at 405 nm was also measured at 37  $^\circ\text{C}$ .

Volumetric enzyme activity EA (U/mL) can be calculated using the time-dependent slope of the absorbance  $dA/dt$  ( $\text{min}^{-1}$ ) according to Equation (5).

$$EA = \frac{\frac{dA}{dt} \cdot V_R}{\varepsilon \cdot d \cdot V_E} \quad (5)$$

$V_R$  is the total volume of the reaction mixture,  $V_E$  is the volume of the enzyme solution,  $\varepsilon$  is the molar extinction coefficient (8.98  $\text{cm}^2/\mu\text{mol}$ ), and  $d$  is the layer thickness of the reaction solution.

## 3. Results and Discussion

### 3.1. Production of Cross-Linked Enzyme Crystals (CLECs) of Different PGAs

For the indentation measurements, cross-linked enzyme crystals (CLECs) have to be immobile and adhered to a flat surface. Therefore, crystallization of the different PGAs was performed on siliconized cover slides to ensure a better adhesion of crystals due to the functionalization. Furthermore, to guarantee a consistent morphology for similar mechanical behavior and a flat surface to perform the indentation with the cantilever tip, the crystal forms were adapted by varying the concentration of the different PGAs (5–10 mg/mL) as well as the concentration and pH (4.6–7.5) of the crystallization buffers. In addition, crystal seeds were used increasing the reproducibility of crystallization and adjusting the crystal size and their numbers in one approach. As the seeds act as nucleation sites for crystal growth, no de novo nucleation was necessary, making crystallization more reproducible [16].

The changes in concentrations and the seeding resulted in faster crystallization and a reproducible crystal morphology for the FJAT-PGA. Furthermore, the number and size of crystals could be influenced by the number of seeds used. A large number gave many

crystals which remained small as the concentration of PGA decreased rapidly due to the large number of crystallization sites (Figure 2a). By reducing the concentration of crystal seeds, the number of crystals decreased while their sizes increased due to a distribution of PGA molecules among fewer crystals (Figure 2b,c). While previous studies have shown that seeding leads to improved hit rates and thus reproducibility in crystallization and improved crystal quality for structure elucidation [24], here it was additionally revealed that crystal number and size can also be adjusted by seeding.



**Figure 2.** FJAT-PGA crystals formed under addition of seeds. Crystals were grown in droplets consisting of 4  $\mu\text{L}$  FJAT-PGA solution (10 mg/mL), 4  $\mu\text{L}$  FJAT-PGA crystallization buffer (8% (*w/v*) PEG 8000 in 100 mM HEPES pH 7.5) and 2  $\mu\text{L}$  of appropriate FJAT-PGA crystal seed suspension (a–c). Seeds were obtained by crushing previously grown FJAT-PGA crystals. (a) No dilution of prepared seeds, (b) addition of a 10-fold diluted seed suspension and (c) addition of a 100-fold diluted seed suspension. The white line represents the scale.

For BtPGA crystallization, the optimization of pH prevented precipitate formation and the use of seeding strategy led to reproducible BtPGA crystals (Figure 3a). Optimized BmPGA crystals were also obtained by seeding. Dilution of seeds in a buffer containing magnesium chloride instead of potassium iodide used in crystallization buffer resulted in an improved crystal morphology (Figure 3b).

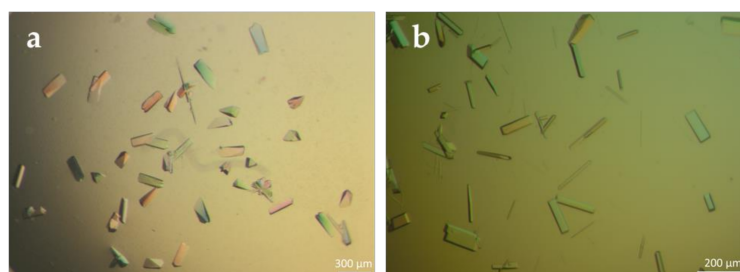


**Figure 3.** Crystals of BtPGA (a) and BmPGA (b). BtPGA crystals formed in droplets containing 4  $\mu\text{L}$  BtPGA solution (6 mg/mL), 4  $\mu\text{L}$  BtPGA crystallization buffer (20 mM calcium chloride, 100 mM sodium acetate (pH 4.6), 30% (*v/v*) MPD, pH 5.57) and 2  $\mu\text{L}$  BtPGA seed suspension. BmPGA crystals developed in 4  $\mu\text{L}$  BmPGA solution (5 mg/mL), 4  $\mu\text{L}$  BmPGA crystallization buffer (200 mM potassium iodide, 20% (*w/v*) PEG 3350) and 2  $\mu\text{L}$  BmPGA seeds diluted in a buffer containing 200 mM magnesium chloride and 20% (*w/v*) PEG 3350. The white line represents the scale.

Subsequently, suited crystals were cross-linked with 5% glutaraldehyde for 24 h to immobilize the different PGAs.

### 3.2. Mechanical Characterization of PGA CLECs

Knowledge of the mechanical properties of CLECs is necessary for potential industrial use to prevent particle breakage and thus ensure long-term stability of CLECs. In order to identify the structure–properties correlation of distinct PGA variants, the corresponding PGA CLECs were examined using an AFM-based nanoindentation method.

Figure 4 provides the cumulative distributions of the hardness and Young's moduli of the investigated PGA CLECs. The hardness of materials is associated with plastic

and elastic deformation mechanisms in a material. Hence, it depends on the structural properties and deformation mechanisms. The FJAT-PGA CLECs showed the highest hardness, with a median of 25.7 MPa, followed by the BmPGA CLECs (22.6 MPa) and the BtPGA CLECs (11.4 MPa). Thus, the BmPGA CLECs showed 12% lower hardness compared to the FJAT-PGA CLECs, while the BtPGA CLECs showed 66% lower hardness. Hardness is also correlated with Young's modulus (or Elastic modulus) in biomaterials [25]. Young's modulus is an intrinsic material property and fundamentally related to atomic bonding. It presents the stiffness of a material, what means how easily it is bended or stretched. The FJAT-PGA CLECs exhibited the highest Young's modulus of the PGAs studied, with a median of 1452 MPa, followed by the BmPGA CLECs (1170 MPa). The BtPGA CLECs possessed the smallest Young's modulus at 614 MPa. Thus, the FJAT-PGA CLECs presented the stiffest and least deformable PGA CLECs, followed by the BmPGA CLECs and the BtPGA CLECs.

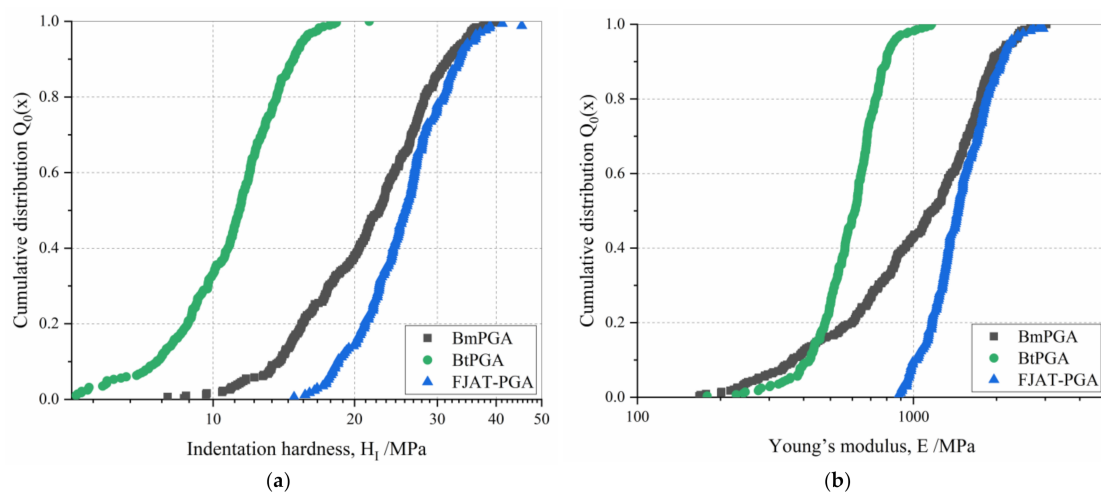


**Figure 4.** Cumulative distribution of hardness (a) and Young's modulus (b) for Bm-, Bt- and FJAT-PGA CLECs determined by AFM nanoindentation. The AFM nanoindentation measurements were performed using a spherical cantilever tip with a radius of 300 nm in a force-controlled mode. The indentations were carried out with an indentation speed of 2  $\mu\text{m/s}$  until an indentation force of 250 nN was reached.

Similar to other particle systems [26–29], CLECs have lognormal distributions as well. However, it can be seen in Figures 4 and 5 that the results of mechanical properties of BmPGA significantly deviate from the lognormal distribution. The varying distribution width of tested PGA CLECs can be additionally seen in Figure 5, which shows differential distributions of hardness using a linear x-axis.

In order to illustrate the variation of mechanical properties of the regarded BmPGA CLECs, all results are plotted as single cumulative distributions of hardness (Figure 6). A detailed analysis of these single face results from BmPGA indicated that all distributions on single crystal faces were relatively narrow, but the discrepancy between the micromechanical properties of the single crystal faces was significant (Figure 6). Looking at the hardness results of single crystal faces, it is noticeable that the distributions were not homogeneous and form gaps. For better visualization, three colored areas in Figure 6 were highlighted. This could indicate that the surfaces of the BmPGA rod-shaped crystals, which can be seen in Figure 3b, have anisotropic properties, even though they appear similar. In particular, at least two groups of hardness distributions can be distinguished in Figure 6, which indicates a minimum of two anisotropic surfaces: the first one (left area, Figure 6) has an average hardness of ca. 14 MPa and the second one (middle area, Figure 6) has a mean hardness of ca. 25 MPa. It is not known whether the single distribution in the area on the right side (right area, Figure 6) represents an outlier or a surface with particularly high mechanical stability. Since the results do not clearly indicate anisotropy, no definite reasons for the wide range of single face measurement results for BmPGA can be given.



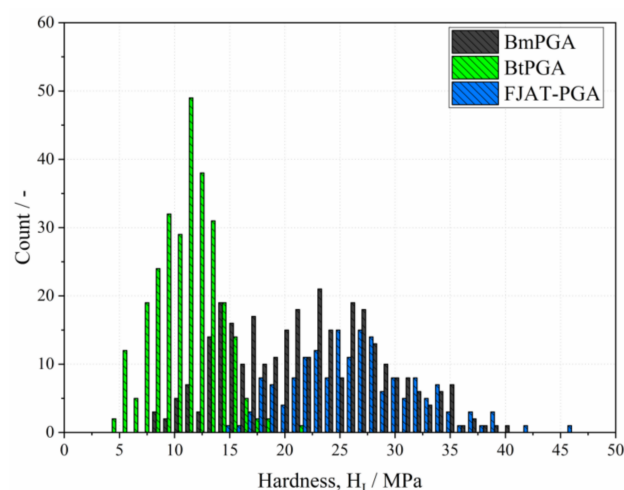


**Figure 5.** Differential distribution of hardness for Bm-, Bt- and FJAT-PGA CLECs determined by AFM nanoindentation.

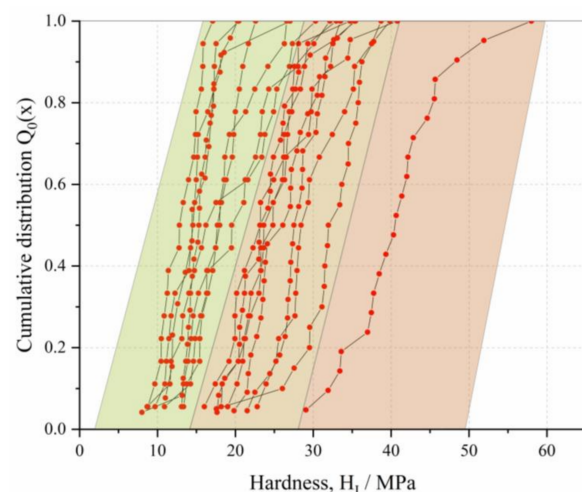


**Figure 6.** Cumulative hardness distribution for single cross-linked crystal faces of BmPGA.

In general, anisotropy is related to the lattice structure of crystals and the intermolecular forces between individual proteins within them. Based on the Protein Data Bank (PDB) file of the crystal structure of BmPGA, it was not possible to assign the molecular packing to the outer crystal face. Therefore, other factors, such as impurities on the surface or dislocations in the crystals, can be considered as possible causes for these results. Additionally, the duration of cross-linking can influence the mechanical properties of CLECs. Kubiak et al. reported that the anisotropy of prismatic faces of halohydrin dehalogenase HheG CLECs occurs when cross-linking duration is insufficient, so that the cross-linking is not completed. The authors state that 24 h are needed for homogeneously cross-linking of HheG crystals [17]. Since in our study the crystals exhibited different sizes, the altered diffusion resistance could have led to different degrees of cross-linking and thus to a broad spectrum of mechanical properties of crystal faces of individual CLECs. Hence, it is possible that anisotropy in BmPGA CLECs could be reduced by longer cross-linking durations. However, taking into account that cross-linking can lead to a reduction in or even loss of catalytic activity [8], a compromise between sufficient but not excessive cross-linking had to be found. Hence, allowing for comparable results, a constant cross-linking time of 24 h was used for all PGA CLECs.

Interestingly, the mechanical stability of the CLECs cannot be correlated with the previously determined thermal stability of the soluble PGAs (Table 1). FJAT-PGA is the most thermally and micromechanically stable PGA. However, the BmPGA CLECs

show only slightly lower mechanical hardness, although BmPGA, with a melting point at 56.8 °C, is significantly less thermostable than FJAT-PGA (73.3 °C). In contrast, BtPGA shows intermediate thermostability (64.5 °C) but the lowest mechanical stability of the measured PGA CLECs [6]. This might be explained by a differing influence of intra- and intermolecular interactions. For thermal stability, intramolecular interactions such as hydrogen bonds or salt bridges within a molecule are mainly responsible for delaying unfolding under heat [30], while for mechanical stability, in addition to intramolecular interactions, intermolecular interactions, especially at crystal contacts, and the arrangement of molecules in the crystal lattice are important. In addition, the mechanical stability can be strongly influenced by the cross-linking with glutaraldehyde [17].

**Table 1.** Properties of FJAT-, Bt- and BmPGA.

	FJAT-PGA CLECs (6NVX) <sup>a</sup>	BtPGA CLECs (6NVY) <sup>a</sup>	BmPGA CLECs (6NVW) <sup>a</sup>
Median hardness (MPa)	26	11	23
Median Young's modulus (MPa)	1452	614	1170
Melting temperature (°C) <sup>b</sup>	74.3	64.5	56.0
Solvent content (%) <sup>c</sup>	54.6	64.8	43.5
Number of symmetry mates (12 Å) <sup>c</sup>	10	8	12
Number of lysine residues <sup>c</sup>	78	49	74

<sup>a</sup> The PDB codes of the structures are given in parentheses [6]. <sup>b</sup> Values of melting temperatures are taken from [6]. <sup>c</sup> Solvent content, number of symmetry mates and of lysine residues were obtained from PDB files 6NVX, 6NVY and 6NVW [6].

To further analyze the differences in the mechanical stability of the three PGA variants, the arrangement of the enzyme molecules in the crystal lattice was investigated using PyMol [31]. Comparison of the arrangement of PGA molecules within the crystals revealed that in the crystals of Bm- and FJAT-PGA the individual molecules are arranged very close to each other and only have small water channels, whereas in the BtPGA crystals significantly larger free spaces between the single molecules can be observed (Figure 7). The distances between the individual molecules are about 2.3 and 2 times larger in the BtPGA crystals compared to Bm- and FJAT-PGA crystals, respectively. Converted to volume, this corresponds to an enlargement of the water channels by factors of 12 and 8 compared to Bm- and FJAT-PGA crystals, respectively. Furthermore, it could be seen that distances and volumes of water channels are 1.2 and 1.9 times larger in FJAT-PGA than in BmPGA crystals.

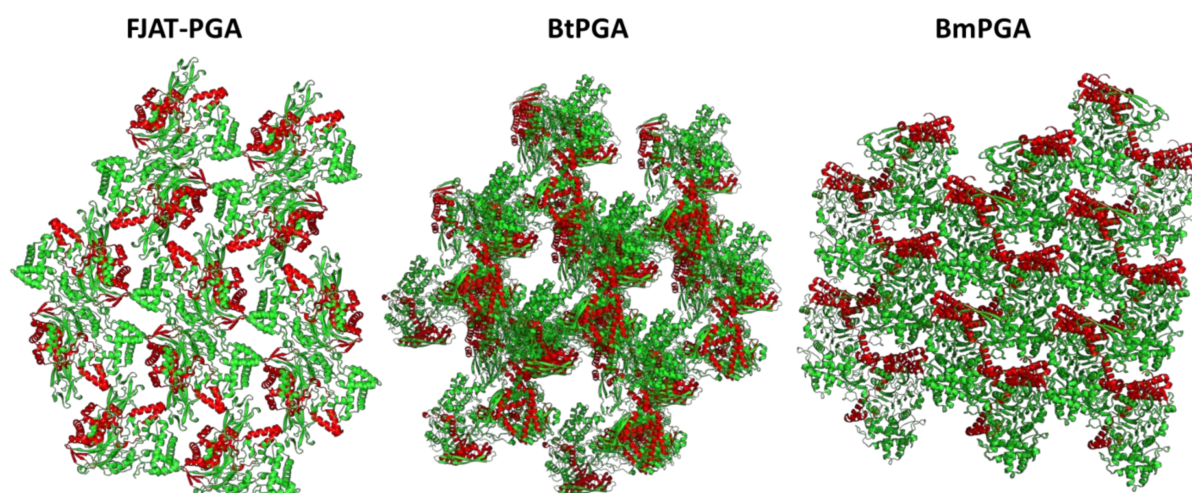


**Figure 7.** Arrangement of symmetry mates 50 Å around the asymmetric unit of FJAT-, Bt- and BmPGA (6NVX, 6NVY and 6NVW from [6]). The  $\alpha$ -subunits are shown in red and the  $\beta$ -subunits in green. This figure was generated using PyMOL [31].

This observation was also reflected in the volume fraction of water (solvent content) and the number of neighboring molecules (symmetry mates) within the crystals (Table 1). The BmPGA crystals show the lowest water content of the PGA crystals studied here (43.5%). One heterodimer is surrounded by 12 other heterodimers, resulting in the highest packing density. In contrast, the BtPGA crystals have a very high solvent content of 64.8%, while that of the FJAT-PGA crystals is 54.6%. According to an evaluation of all PDB structures published until February 2007, the mean solvent content of all structures is 51% [32]. Possibly, the BtPGA CLECs exhibit lower stabilities than CLECs of FJAT- and BmPGA due to a high solvent content that is significantly above average, while the solvent content of the BmPGA CLECs below the average does not seem to cause further increase in stability when compared to FJAT-PGA CLECs with average solvent content.

Additionally, the mechanical behavior of the PGA CLECs could be influenced by the covalent cross-linking using glutaraldehyde by which mainly lysine residues were cross-linked [33]. The BtPGA heterodimer has 49 lysine residues, whereas FJAT- and BmPGA possess significantly higher numbers of lysine residues—78 and 74, respectively (Table 1). Hence, the lower hardness values of BtPGA CLECs, only 44.4 and 50.4%, respectively, compared to those of FJAT- and BmPGA CLECs might be also caused by the lower number of lysine residues available for cross-linking events.

When comparing these results with previously published micromechanical properties of CLECs of halohydrin dehalogenase HheG and lysozyme also measured with the AFM-based nanoindentation technique (Table 2) [16,17], the PGA CLECs were found to be more stable. FJAT-PGA CLECs (26 MPa) and BmPGA CLECs (23 MPa) are about twice as hard as lysozyme and HheG CLECs, while the hardness values of BtPGA, HheG, and lysozyme CLECs are similar. The solvent content of HheG crystals (65%) is similar to that of BtPGA crystals (64.8%). In combination with the low number of lysine residues of only 0.17 kDa<sup>-1</sup>, HheG also appears to have a reduced mechanical stability. With 40.5%, the lysozyme crystals have the lowest solvent content, but did not show correspondingly high stability. Possibly, the lower number of lysine residues (0.42 kDa<sup>-1</sup>) compared to those of FJAT- and BmPGA (0.90 kDa<sup>-1</sup>, 0.86 kDa<sup>-1</sup>) contributed to this result. However, the lysozyme CLECs were cross-linked for less time (~12 h) [16]. Maybe a greater hardness would have been observed with a cross-linking time of 24 h as for HheG CLECs, increasing the cross-linking time from 4 to 24 h resulted in a threefold increase in hardness [17].

**Table 2.** Micromechanical and crystal properties of FJAT-, Bt- and BmPGA CLECs as well as HheG and lysozyme CLECs.

	FJAT-PGA CLECs (6NVX) <sup>a</sup>	BtPGA CLECs (6NVY) <sup>a</sup>	BmPGA CLECs (6NVW) <sup>a</sup>	HheG CLECs (5O30) <sup>a</sup>	Lysozyme CLECs (3LYZ) <sup>a</sup>
Median hardness (MPa)	26	11	23	Prismatic face: 11 <sup>b</sup> , Basal face: 14.5 <sup>b</sup>	12 <sup>b</sup>
Median Young's modulus (MPa)	1452	614	1170	Prismatic face: 500 <sup>b</sup> , Basal face: not shown <sup>b</sup>	1073 <sup>b</sup>
Solvent content (%)	54.6	64.8	43.5	65.0	40.5
Number of lysine residues per molecular weight (kDa <sup>-1</sup> )	0.90	0.57	0.86	0.17	0.42
Space group	P2 <sub>1</sub> 2 <sub>1</sub> 2 <sub>1</sub>	H3	P2 <sub>1</sub>	P3 <sub>1</sub> 21	P4 <sub>3</sub> 2 <sub>1</sub> 2
Crystal system	orthorhombic	hexagonal	monoclinic	trigonal	tetragonal

<sup>a</sup> The PDB codes of the structures are given in parentheses [6,34,35]. <sup>b</sup> Median hardness and Young's modulus of HheG CLECs from [17] and of lysozyme CLECs of [16].

Furthermore, it can be seen that all five proteins compared here crystallized in different space groups and crystal systems (Table 2). The above-mentioned evaluation of all PDB structures published until February 2007 show that the average solvent content of crystals varies depending on the crystal system [32]. The average solvent contents of orthorhombic and monoclinic crystals, such as FJAT-PGA and BmPGA crystals, with 49 and 48%, respectively, were significantly lower than the average solvent content of hexagonal (57%), trigonal (55%), and tetragonal crystals (56%) [32]. This could also be confirmed for the crystals studied and compared here, except for lysozyme. It is possible that the packing density of lysozyme is particularly high due to its low molecular weight

of 14.31 kDa and thus the solvent content is lower. By analyzing the behaviors of CLECs of further enzymes, it could be investigated whether there is a significant dependence between water content, crystal shape and mechanical properties. Lysozyme could also be studied as a model protein, since lysozyme crystals have already been obtained in different crystal systems [36].

### 3.3. Activity of PGA CLECs

As the activity of CLECs is also essential for a possible application as immobilized biocatalyst, the activity of the PGA CLECs was determined. In previous studies it was also shown that enzymes in the crystalline and cross-linked state were still active but lost activity compared to soluble enzyme. For example, carboxypeptidase A CLECs exhibited around 30% residual activity compared to the free enzyme due to the chemical cross-linking reaction and diffusion limitation [37]. Furthermore, CLECs of PGA from *E. coli* showed between 21 and 71% residual activity [9]. However, soluble FJAT-, Bt- and BmPGA used here showed 4.5, 3.5 and 3.9 times higher activities compared to soluble PGA from *E. coli* in our experiments, respectively. Therefore, FJAT-, Bt- and BmPGA provide promising alternatives to PGA from *E. coli*.

Activities of PGA CLECs analyzed here were determined using the same assay as for activity determination of free PGA enzyme [6]. For this, CLECs from a 10  $\mu$ L approach were rinsed with reaction solution from the cover slide into a flat-bottom microtiter plate and the absorbance was measured. For FJAT- and BtPGA CLECs, an increasing absorbance was observed, which clearly showed activity of the FJAT- and BtPGA CLECs. However, BmPGA CLECs showed a reduced activity of only 5% when compared to FJAT- and BtPGA CLECs. The low activity might be caused by high diffusion limitations in BmPGA CLECs due to high packing density and low solvent content of the BmPGA crystal (Figure 6, Table 1). Furthermore, cross-linking near the active site might have further narrowed the water channels.

The higher volumetric activities of FJAT- and BtPGA CLECs offer a better potential for a possible application. However, the determined volumetric activity differed for the individually measured CLEC samples due to an inconstant amount of crystals rinsed from the cover slide. Nevertheless, it could be observed that average activity was higher for FJAT-PGA CLECs than for BtPGA CLECs. The native FJAT-PGA also showed the highest specific activity of 13.7 U/mg when applied as a free enzyme using the same reaction conditions. With 10.6 and 12.0 U/mg, respectively, free BtPGA and BmPGA showed slightly reduced activities. Due to a higher solvent content and larger water channels, a better diffusion of substrate and product was expected for BtPGA crystals. However, the influence of the individual factors remained unclear. Within this study, the exact mass of the CLECs used could not be accurately calculated due to their small dimensions. Scaling up of production, purification, crystallization, CLEC formation and analysis will be subject of future studies.

## 4. Conclusions

This study was designed for the production and characterization of cross-linked enzyme crystals (CLECs) at a small scale. We used industrially relevant enzymes, FJAT-, Bt- and BmPGA, characterized by similar crystal structures. Despite this similarity, the PGAs behaved completely differently along the entire process chain. During crystallization, it was noticed that conditions, morphologies and space groups of the PGA crystals differed. With the AFM-based nanoindentation technique, the smallest changes at the nanometer scale could be detected showing highest hardness (~26 MPa) and Young's modulus (1450 MPa) for FJAT-PGA CLECs, followed by BmPGA (23 MPa/1170 MPa) and BtPGA CLECs (11 MPa/614 MPa). The different material behavior could be partly correlated with properties such as solvent content, degree of cross-linking or amount of amino acid residues involved in glutaraldehyde cross-linking. High solvent content and low amount of lysine residues within the enzyme might lead to lower stability.



Our results clearly indicate that the production of CLECs can and should be individually adapted to each respective enzyme. For this, knowledge of mechanical behavior of CLECs at a small scale as presented here can provide a better understanding of the underlying mechanisms and thus reduce the number of experiments to establish a biotechnological process. This can be followed by future research on mechanical and catalytical behavior of CLECs in biotechnological applications demanding larger amounts of CLECs. Therefore, a scale-up of crystallization by establishment of, e.g., precipitation crystallization instead of vapor diffusion crystallization could be performed. Thereby, the investigation of crystal slurries instead of single crystals should be possible. The investigation of mechanical properties of crystal slurries in a shear cell, filtration system or stirred tank reactor can probably provide further valid conclusions about the robustness of special CLECs in production processes, as interactions of several CLECs can be measured. The study of crystal slurries at a milliliter scale would also allow reliable measurements and determination of accurate data of catalytic activity.

**Supplementary Materials:** The following are available online at <https://www.mdpi.com/article/10.3390/cryst11040451/s1>, Table S1: Summary of mechanical properties of CLECs

**Author Contributions:** M.K. and J.M. contributed equally to this study; conceptualization, M.K., J.M., I.K., C.S., and R.B.; data curation, M.K. and J.M.; funding acquisition, C.S. and R.B.; investigation, M.K. and J.M.; methodology, M.K. and J.M.; project administration, I.K.; supervision, I.K., C.S., and R.B.; writing—original draft, M.K. and J.M.; writing—review and editing, C.S. and R.B. All authors have read and agreed to the published version of the manuscript.

**Funding:** This work was funded by the German Research Foundation (DFG), within the priority program SPP1934 “Dispersitäts-, Struktur- und Phasenänderungen von Proteinen und biologischen Agglomeraten in biotechnologischen Prozessen”.

**Institutional Review Board Statement:** Not applicable.

**Informed Consent Statement:** Not applicable.

**Data Availability Statement:** The data presented in this study are available within the article.

**Acknowledgments:** We acknowledge financial support by the German Research Foundation and the Open Access Publication Funds of the Technische Universität Braunschweig.

**Conflicts of Interest:** The authors declare no conflict of interest.

## References

1. Marešová, H.; Plačková, M.; Grulich, M.; Kyslík, P. Current state and perspectives of penicillin G acylase-based biocatalyses. *Appl. Microbiol. Biotechnol.* **2014**, *98*, 2867–2879. [[CrossRef](#)] [[PubMed](#)]
2. Bush, K.; Bradford, P.A.  $\beta$ -Lactams and  $\beta$ -Lactamase Inhibitors: An Overview. *Cold Spring Harb. Perspect. Med.* **2016**, *6*, a025247. [[CrossRef](#)] [[PubMed](#)]
3. Basso, A.; Serban, S. Industrial applications of immobilized enzymes—A review. *Mol. Catal.* **2019**, *479*, 110607. [[CrossRef](#)]
4. Rajendhran, J.; Gunasekaran, P. Recent biotechnological interventions for developing improved penicillin G acylases. *J. Biosci. Bioeng.* **2004**, *97*, 1–13. [[CrossRef](#)]
5. Cobos-Puc, L.; Rodríguez-Herrera, R.; Cano-Cabrera, J.C.; Aguayo-Morales, H.; Silva-Belmares, S.Y.; Flores Gallegos, A.C.; Martínez Hernández, J.L. Classical and New Pharmaceutical Uses of Bacterial Penicillin G Acylase. *Curr. Pharm. Biotechnol.* **2020**, *21*, 287–297. [[CrossRef](#)] [[PubMed](#)]
6. Mayer, J.; Pippel, J.; Günther, G.; Müller, C.; Lauer mann, A.; Knuuti, T.; Blankenfeldt, W.; Jahn, D.; Biedendieck, R. Crystal structures and protein engineering of three different penicillin G acylases from Gram-positive bacteria with different thermostability. *Appl. Microbiol. Biotechnol.* **2019**, *103*, 7537–7552. [[CrossRef](#)] [[PubMed](#)]
7. Sheldon, R.A.; van Pelt, S. Enzyme immobilisation in biocatalysis: Why, what and how. *Chem. Soc. Rev.* **2013**, *42*, 6223–6235. [[CrossRef](#)] [[PubMed](#)]
8. Margolin, A.L. Novel crystalline catalysts. *Trends Biotechnol.* **1996**, *14*, 223–230. [[CrossRef](#)]
9. Margolin, A.L.; Navia, M.A. Protein Crystals as Novel Catalytic Materials. *Angew. Chem. Int. Ed.* **2001**, *40*, 2204–2222. [[CrossRef](#)]
10. Koizumi, H.; Kawamoto, H.; Tachibana, M.; Kojima, K. Effect of intracrystalline water on micro-Vickers hardness in tetragonal hen egg-white lysozyme single crystals. *J. Phys. D Appl. Phys.* **2008**, *41*, 074019. [[CrossRef](#)]
11. Tachibana, M.; Kobayashi, Y.; Shimazu, T.; Ataka, M.; Kojima, K. Growth and mechanical properties of lysozyme crystals. *J. Cryst. Growth* **1999**, *198–199*, 661–664. [[CrossRef](#)]



12. Suzuki, R.; Kishi, T.; Tsukashima, S.; Tachibana, M.; Wako, K.; Kojima, K. Hardness and slip systems of orthorhombic hen egg-white lysozyme crystals. *Philos. Mag.* **2016**, *96*, 2930–2942. [[CrossRef](#)]
13. Kishi, T.; Suzuki, R.; Shigemoto, C.; Murata, H.; Kojima, K.; Tachibana, M. Microindentation Hardness of Protein Crystals under Controlled Relative Humidity. *Crystals* **2017**, *7*, 339. [[CrossRef](#)]
14. Tait, S.; White, E.T.; Litster, J.D. Mechanical Characterization of Protein Crystals. *Part. Part. Syst. Charact.* **2008**, *25*, 266–276. [[CrossRef](#)]
15. Morozov, V.N.; Morozova, T.Y. Viscoelastic properties of protein crystals: Triclinic crystals of hen egg white lysozyme in different conditions. *Biopolymers* **1981**, *20*, 451–467. [[CrossRef](#)]
16. Kubiak, M.; Solarczek, J.; Kampen, I.; Schallmeyer, A.; Kwade, A.; Schilde, C. Micromechanics of anisotropic cross-linked enzyme crystals. *Cryst. Growth Des.* **2018**, *18*, 5885–5895. [[CrossRef](#)]
17. Kubiak, M.; Storm, K.F.; Kampen, I.; Schilde, C. Relationship between Cross-Linking Reaction Time and Anisotropic Mechanical Behavior of Enzyme Crystals. *Cryst. Growth Des.* **2019**, *19*, 4453–4464. [[CrossRef](#)]
18. Wittchen, K.D.; Meinhardt, F. Inactivation of the major extracellular protease from *Bacillus megaterium* DSM319 by gene replacement. *Appl. Microbiol. Biotechnol.* **1995**, *42*, 871–877. [[CrossRef](#)]
19. Lakowitz, A.; Krull, R.; Biedendieck, R. Recombinant production of the antibody fragment D1.3 scFv with different *Bacillus* strains. *Microb. Cell Fact.* **2017**, *16*, 1–18. [[CrossRef](#)]
20. Bradford, M.M. A rapid and sensitive method for quantitation of microgram quantities of protein utilizing the principle of protein-dye-binding. *Anal. Biochem.* **1976**, *72*, 248–254. [[CrossRef](#)]
21. Tranchida, D.; Piccarolo, S.; Loos, J.; Alexeev, A. Mechanical Characterization of Polymers on a Nanometer Scale through Nanoindentation. A Study on Pile-up and Viscoelasticity. *Macromolecules* **2007**, *40*, 1259–1267. [[CrossRef](#)]
22. Oliver, W.C.; Pharr, G.M. Measurement of hardness and elastic modulus by instrumented indentation: Advances in understanding and refinements to methodology. *J. Mater. Res.* **2004**, *19*, 3–20. [[CrossRef](#)]
23. Fischer-Cripps, A.C. *Nanoindentation*, 3rd ed.; Mechanical Engineering Series; Springer: New York, NY, USA, 2011; ISBN 978-1-4419-9871-2.
24. D’Arcy, A.; Bergfors, T.; Cowan-Jacob, S.W.; Marsh, M. Microseed matrix screening for optimization in protein crystallization: What have we learned? *Acta Crystallogr. Sect. F Struct. Biol. Commun.* **2014**, *70*, 1117–1126. [[CrossRef](#)] [[PubMed](#)]
25. Labonte, D.; Lenz, A.-K.; Oyen, M.L. On the relationship between indentation hardness and modulus, and the damage resistance of biological materials. *Acta Biomater.* **2017**, *57*, 373–383. [[CrossRef](#)]
26. Schilde, C.; Westphal, B.; Kwade, A. Effect of the primary particle morphology on the micromechanical properties of nanostructured alumina agglomerates. *J. Nanopart. Res.* **2012**, *14*, 745. [[CrossRef](#)]
27. Schilde, C.; Kwade, A. Measurement of the micromechanical properties of nanostructured aggregates via nanoindentation. *J. Mater. Res.* **2012**, *27*, 672–684. [[CrossRef](#)]
28. Arfsten, J.; Kampen, I.; Kwade, A. Mechanical testing of single yeast cells in liquid environment: Effect of the extracellular osmotic conditions on the failure behavior. *Int. J. Mater. Res.* **2009**, *100*, 978–983. [[CrossRef](#)]
29. Arfsten, J.; Bradtmöller, C.; Kampen, I.; Kwade, A. Compressive testing of single yeast cells in liquid environment using a nanoindentation system. *J. Mater. Res.* **2008**, *23*, 3153–3160. [[CrossRef](#)]
30. Xu, Z.; Cen, Y.K.; Zou, S.P.; Xue, Y.P.; Zheng, Y.G. Recent advances in the improvement of enzyme thermostability by structure modification. *Crit. Rev. Biotechnol.* **2020**, *40*, 83–98. [[CrossRef](#)]
31. *The PyMOL Molecular Graphics System*; Version 2.0 Schrödinger; LLC: New York, NY, USA.
32. Chruszcz, M.; Potrzebowski, W.; Zimmerman, M.D.; Grabowski, M.; Zheng, H.; Lasota, P.; Minor, W. Analysis of solvent content and oligomeric states in protein crystals—does symmetry matter? *Protein Sci.* **2008**, *17*, 623–632. [[CrossRef](#)]
33. Yan, E.K.; Cao, H.L.; Zhang, C.Y.; Lu, Q.Q.; Ye, Y.J.; He, J.; Huang, L.J.; Yin, D.C. Cross-linked protein crystals by glutaraldehyde and their applications. *RSC Adv.* **2015**, *5*, 26163–26174. [[CrossRef](#)]
34. Diamond, R. Real-space refinement of the structure of hen egg-white lysozyme. *J. Mol. Biol.* **1974**, *82*, 371–391. [[CrossRef](#)]
35. Koopmeiners, J.; Diederich, C.; Solarczek, J.; Voß, H.; Mayer, J.; Blankenfeldt, W.; Schallmeyer, A. HheG, a Halohydrin Dehalogenase with Activity on Cyclic Epoxides. *ACS Catal.* **2017**, *7*, 6877–6886. [[CrossRef](#)]
36. Elgersma, A.V.; Ataka, M.; Katsura, T. Kinetic studies on the growth of three crystal forms of lysozyme based on the measurement of protein and Cl<sup>-</sup> concentration changes. *J. Cryst. Growth* **1992**, *122*, 31–40. [[CrossRef](#)]
37. Quiocho, F.A.; Richards, F.M. Intermolecular cross linking of a protein in the crystalline state: Carboxypeptidase-A. *Proc. Natl. Acad. Sci. USA* **1964**, *52*, 833–839. [[CrossRef](#)]